Available online at www.sciencedirect.com
SCIENCE DIRECT®
Biochemical and Biophysical Research Communications 335 (2005) 631–636
BBRC
www.elsevier.com/locate/ybbrc

Lib, transcriptionally induced in senile plaque-associated astrocytes, promotes glial migration through extracellular matrix

Kazuki Satoh [a,*], Mitsumi Hata [a], Tomoko Shimizu [a], Hiroshi Yokota [b], Hiroyasu Akatsu [c], Takayuki Yamamoto [c], Kenji Kosaka [c], Tatsuo Yamada [d]

[a] *The Fifth Frontier Project, Daiichi Pharmaceutical Co., Ltd., Tokyo 134-8640, Japan*
[b] *Drug Discovery Research Laboratory, Daiichi Pharmaceutical Co., Ltd., Tokyo 134-8640, Japan*
[c] *Choju Medical Institute, Fukushimura Hospital, Aichi 441-8124, Japan*
[d] *Fifth Department of Internal Medicine, Fukuoka University, Fukuoka 814-0180, Japan*

Received 12 July 2005
Available online 10 August 2005

Abstract

In an effort to identify astrocyte-derived molecules that may be intimately associated with progression of Alzheimer's disease (AD), Lib, a type I transmembrane protein belonging to leucine-rich repeat superfamily, has been identified as a distinctly inducible gene, responsive to β-amyloid as well as pro-inflammatory cytokines in astrocytes. To evaluate the roles of Lib in AD, we investigated Lib expression in AD brain. In non-AD brain, Lib mRNA has been detected in neurons but not in quiescent astrocytes. On the contrary, in AD brain, Lib mRNA is expressed in activated astrocytes associated with senile plaques, but not expressed in neurons around lesions. Lib-expressing glioma cells displayed promotion of migration ability through reconstituted extracellular matrix and recombinant Lib protein bound to constituents of extracellular matrix. These observations suggest that Lib may contribute to regulation of cell–matrix adhesion interactions with respect to astrocyte recruitment around senile plaques in AD brain.

Keywords: LRR; mRNA expression; Alzheimer's disease; Cellular migration; Extracellular matrix

Neuropathological changes in the brains from patients with Alzheimer's disease (AD) include loss of neurons, intracellular formation of neurofibrillary tangles, appearance of numerous β-amyloid (Aβ)-containing amyloid plaques, as well as reactive gliosis. Numerous reactive astrocytes observed in lesions are a common feature of an AD brain as well as in many other neurodegenerative disorders. They surround senile plaques and have morphological changes, extending processes into the lesions and producing a variety of inflammatory mediators [1–5]. These observations support the notion that the activated astrocytes in AD lesions have a significant influence on the neighboring neurons and their environment, leading to exacerbation of the disease.

In efforts to identify key molecules from astrocytes intimately involved in the disease, Lib (an LRR protein induced by β-amyloid treatment) was identified as a distinctly inducible gene, responsive to Aβ as well as to pro-inflammatory cytokines in astrocytes [6]. Lib protein is a type I transmembrane protein with an extracellular domain consisting of 15 leucine-rich repeats (LRRs) flanked by both N- and C-terminal cysteine-rich regions that form intramolecular disulfide loops, similar to the extracellular binding motifs of some adhesion proteins and receptors [7–9]. Lib is thought to play a role in inflammatory states via the LRR motif, an ideal structural framework for specific protein–protein and/or protein–matrix interactions including adhesion, target recognition or receptor–ligand binding [6–10].

In this study, the distribution of Lib mRNA expression in AD brain was evaluated to give insight into the

* Corresponding author. Fax: +81 3 5696 8196.
E-mail address: satohj7i@daiichipharm.co.jp (K. Satoh).

0006-291X/$ - see front matter © 2005 Elsevier Inc. All rights reserved.
doi:10.1016/j.bbrc.2005.07.117

pathological involvement of Lib. Based on the observation that Lib is expressed in plaque-associated activated astrocytes, the functional involvement of Lib in glial migration through extracellular matrix (ECM) was analyzed. Although interactions between ECM macromolecules and astrocytes are required in migrating towards and remaining around the AD lesions, molecular mechanisms involved with these events are not well understood. Our results suggest that Lib may participate in astroglial motility around senile plaques in AD brain.

Materials and methods

Brains. The brains were obtained from the brain bank of the Choju Medical Institute of Fukushimura Hospital and protocols used were approved by the Ethics Committee of Fukushimura Hospital. The scientific use of this human material was conducted in accordance with the Declaration of Helsinki and informed consents were obtained from the guardians of the patients. The brains from five neurologically normal control patients in which Alzheimer's disease (AD)-type changes were lacking, and those from five patients with AD were examined. The diagnosis of AD was established using the criteria recommended by the National Institute on Aging [11] and the Consortium to Establish a Registry for Alzheimer's Disease (CERAD) [12]. The ages of the three male and two female neurologically normal controls ranged from 54 to 82 years, and those of the two male and three female patients with AD from 67 to 80 years. In all cases, brains were obtained within 2–13 h after death. Small blocks were dissected from the parietal lobes and stored at −80 °C until used. The frozen samples were thawed and fixed for 2 days in phosphate-buffered 4% paraformaldehyde. They were then transferred to a maintenance solution of 15% sucrose in 0.1 M phosphate buffer, pH 7.4, and kept in the cold until used. Sections were cut on a freezing microtome at 20-μm thickness.

In situ hybridization. Human Lib expression in AD brain tissue was evaluated by in situ hybridization histochemistry. Human Lib cDNA fragments, encompassing nucleotides 1444–1742 of hLib open-reading frame (ORF; Accession No. AB071037), were amplified by PCR and cloned into pCR-Blunt II-TOPO (Invitrogen). A cDNA probe for hLib was constructed by PCR using T7 and SP sequences in the vector as primers. Amplifications were done in 100 μl PCR buffer containing 10 pM primer, 2 nM dNTPs, 200 pM digoxigenin-11-dUTP (Roche), 10 ng template plasmid, and 5 U Ampli-Taq DNA polymerase using a thermal cycler (Perkin-ElmerGeneAmp PCR System 9600). Samples were denatured at 94 °C for 5 min, followed by 30 cycles of amplification for 30 s at 94 °C, for 30 s at 50 °C, and for 30 s at 72 °C. The final extension was at 72 °C for 5 min. Sections were hybridized at 37 °C for 2 days in buffer containing 50% formamide, 4× SSC, 0.2× Denhardt's solution, 21 ng/ml salmon sperm DNA, and 250 ng/ml digoxigenin-11-dUTP labeled and non-labeled PCR DNA probes. After hybridization, sections were rinsed three times in 1× SSC. Hybridization was detected by an enzyme-catalyzed color reaction using the DIG Nucleic Acid Detection kit (Boehringer–Mannheim Biochemica) according to the supplier's instructions. Negative controls were pretreated with RNAase and processed with identical procedures. Other control experiments were done using mixtures of either 10:1 or 1:1 of the digoxigenin-11dUTP-labeled and non-labeled PCR DNA probes. After detection of the mRNA signal for hLib by in situ hybridization, immunohistochemistry [13] was used to characterize the labeled cells using antibody against anti-glial fibrillary acidic protein (GFAP) (1:10,000, rabbit polyclonal, Dako). The sections were mounted on glass slides and the coverslips were sealed with liquid paraffin.

Cell culture and transfection. Human glioma cells were purchased from the American Type Culture Collection. U87MG cells were maintained in Eagle's minimum essential medium (EMEM; Gibco) supplemented with non-essential amino acids (Gibco), pyruvate, and 10% fetal calf serum (FCS; Gibco) at 37 °C under 5% CO_2. H4 cells were cultured in Dulbecco's modified Eagle's medium (DMEM; Gibco) containing 10% FCS. The cells were transfected either with phLib-FLAG plasmid harboring the open-reading frame (ORF) of hLib tagged with a FLAG epitope at the carboxyl terminus or with control empty vector (pCMV-Tag4; Stratagene) using FuGene 6 (Roche). Stably transfected cells expressing hLib and control mock cells were selected with G418 (400 μg/ml; Gibco) for 6 weeks and then obtained as mixed cell lines to avoid clonal variability.

Western blot analysis. Cells were washed with ice-cold phosphate-buffered saline (PBS) and lysed by incubation in lysis buffer (1% NP-40, 150 mM NaCl, 20 mM Hepes, pH 7.5, and complete protease inhibitor cocktail (Roche)) on ice for 30 min. Clarified lysates were obtained by centrifugation (30 min, 15,000*g*, 4 °C). Supernatants were boiled with SDS sample buffer (5 min), separated on a 4–12% sodium dodecyl sulfate–polyacrylamide gel (Novex), and transferred to a polyvinylidene fluoride (PVDF) membrane (NEN). Membranes were immersed for 1 h in blocking solution (5% non-fat dried milk in PBS containing 0.1% Tween 20 (PBS-T)) and probed with a polyclonal antibody raised against hLib (1:2000) in blocking solution overnight at 4 °C. The membranes were washed extensively in PBS-T and incubated with horseradish peroxidase (HRP)-conjugated anti-rabbit IgG antibody (Amersham, 1:3000) in PBS-T at room temperature for 1 h. FLAG-tagged proteins were detected by M2 anti-FLAG antibody (1:2000, Sigma) in blocking solution overnight at 4 °C. Blots were washed and visualized with enhanced chemiluminescence (ECL; Amersham). The actin antibody (Sigma; AC-40) was used as a loading control.

Transmigration analysis. The role of Lib in cellular motility migration through reconstituted extracellular matrix (ECM) was investigated using BioCoat Matrigel 24-well invasion chambers (Becton–Dickinson) according to the supplier's instructions. Cell suspensions (0.5 ml of 5×10^4 cells/ml in 10% FCS-containing medium) were plated onto Matrigel-coated filters in triplicate wells of an invasion chamber. After the 22 h incubation, non-transmigration cells remaining on the upper surface of the filter were removed with a cotton swab and the invasive cells on the under surface were fixed and stained with Diff-Quick staining kit (Kokusai Shiyaku). The cells were photographed at 100× magnification in five predetermined fields and counted.

Blot overlay binding analysis. For production of recombinant hLib protein from sf9 cells (Invitrogen), the extracellular region of hLib (aa 1–529) tagged with His6 at C-terminal was cloned into the pFastBac1 vector (Gibco). The recombinant baculovirus was obtained according to manufacturer's guidelines. Recombinant hLib protein was affinity purified from cultured supernatants of infected sf9 cells using HiTrap Chelating HP (Amersham). Ability of hLib to bind to Matrigel (Becton–Dickinson, 356237), collagen type IV (Becton–Dickinson, 354245), laminin (Becton–Dickinson, 354232), fibronectin (Becton–Dickinson, 354008), aggrecan (Sigma, A1960), and bovine serum albumin (Sigma, A2153) was determined as previously described [14] with slight modifications. Briefly, each macromolecule was spotted onto a PVDF membrane at 5 μg and 0.5 μg/spot. The membrane was incubated with blocking solution at room temperature for 2 h and then incubated with recombinant hLib protein (1 μg/ml) in blocking solution for 16 h at 4 °C. The membrane was incubated with anti-hLib polyclonal antibody (1:1000) for 16 h at 4 °C, followed by extensive washing, incubation with HRP-conjugated anti-rabbit IgG antibody (1:2000; Amersham), and detection with ECL (Amersham).

Results

Lib expression in activated astrocytes adjacent to senile plaques of Alzheimer's disease brain

To evaluate pathological involvement of Lib in AD, localization of hLib gene transcripts was evaluated in cerebral cortex sections from the patients by in situ hybridization analysis. As shown in Fig. 1A, mRNA for hLib was expressed in only neurons, but not in astrocytes in age-matched non-AD cortex sections. In AD brain sections, there appeared areas where hLib mRNA expression was not observed in neurons (Fig. 1B, lower central part) and these areas are thought to be damaged. In these 'neuron-negative' areas, hLib mRNA was detected in some cells surrounding the non-specifically stained senile plaques (Fig. 1C). Immunohistochemistry using an anti-GFAP antibody revealed that these hLib mRNA-positive cells were reactive astrocytes. As shown in Fig. 1D, GFAP-positive astrocytes directly surrounding and extending their processes toward non-specifically faintly stained senile plaques expressed hLib mRNA. Review of five AD brain sections indicated that approximately half of the reactive astrocytes around senile plaques were positive for hLib mRNA expression. Control hybridization sections which were incubated without the DNA probe or with a 1:1 mixture of the digoxigenin-11dUTP-labeled and non-labeled PCR DNA probe were negative. When a 10:1 mixture of the digoxigenin-11dUTP-labeled and non-labeled PCR DNA probe was used, only a weak signal could be detected (data not shown).

Lib promotes glial migration ability through ECM

Cell surface LRR proteins appear to have abilities to interact with extracellular proteins and/or matrixes [7–9]. The observation that Lib is expressed in reactive astrocytes around AD senile plaques (Fig. 1) prompted us to evaluate a role of Lib in cellular migration through ECM. The hLib expression plasmid, harboring hLib ORF with FLAG epitope tag at the C-terminus, was introduced into U87MG and H4 human glial cell lines. Human Lib expression from transfected cells was verified by Western blot analyses using an antibody raised against hLib and M2 anti-FLAG antibody. As shown in Fig. 2A, hLib protein was expressed in established cell lines, while hLib expression was undetectable in both parental wild type and empty vector control lines. The bands observed near 64 kDa are thought to correspond to immature molecules before complete glycosylation [10]. These cells were examined by migration analysis using Matrigel invasion chambers. Human Lib expression promoted migration through Matrigel in both transfected

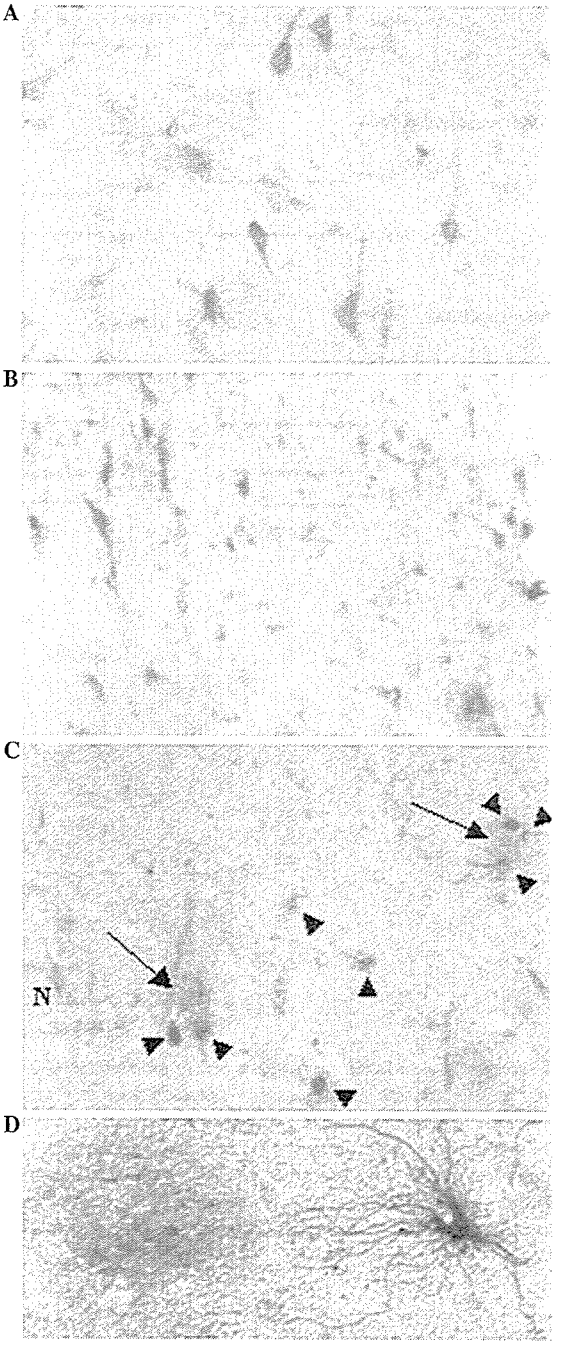

Fig. 1. In situ localization of hLib mRNA in non-AD (A) and AD brain sections (B–D). (A) Positive signals for hLib mRNA were seen in neurons in non-AD cerebral cortex. (B) In AD brain, neurons positive for hLib mRNA expression were observed, similar to non-AD brain. However, unlike non-AD brain, areas devoid of hLib mRNA expression in neurons were observed (lower central part). (C) In an area where hLib mRNA-positive neurons were not seen, signals for hLib mRNA were seen in several other non-neuronal cells (arrowheads). Some positive cells surrounding non-specifically stained senile plaques (arrows) were observed. A neuron with damaged morphology was faintly stained (N). Non-specific staining was seen in some vessels. (D) In situ hybridization histochemistry for hLib mRNA (blue-black) followed by immunohistochemistry with anti-GFAP antibody (brown) in AD brain. Human Lib mRNA-positive cell, that directly surrounded and extended processes toward the non-specifically faintly stained senile plaque, also expressed GFAP. (A–C) 185×; (D) 256×.

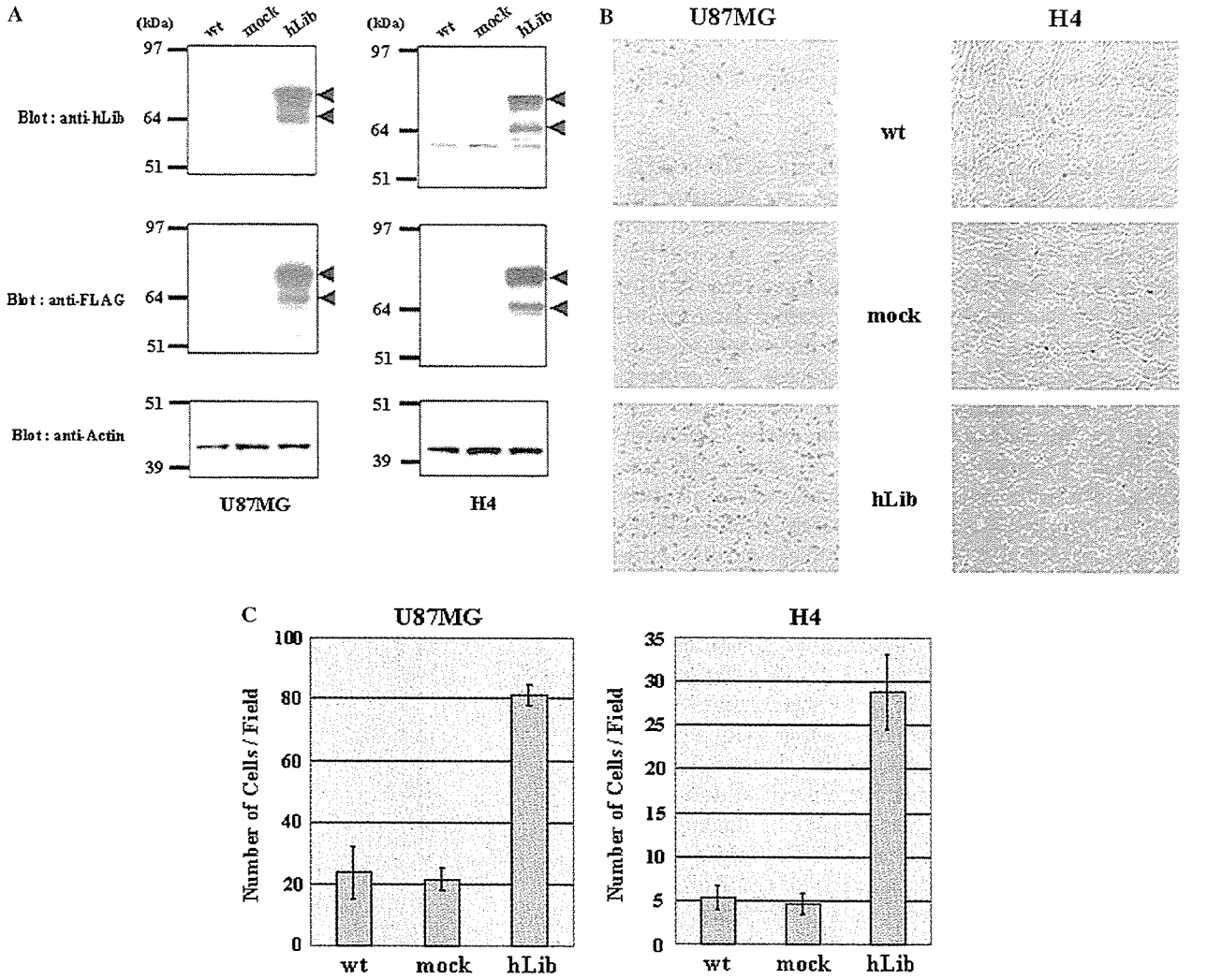

Fig. 2. Acceleration of cell migration by hLib expression. (A) Expression of hLib in transfected U87MG (left panels) or H4 (right panels) cells were detected by Western blot analysis using polyclonal antibody raised against hLib (top panels) or M2 anti-FLAG antibody (middle panels). Anti-hLib antibody reacted with hLib gene products (arrowheads) only in hLib-transfected cells (hLib) and not in parental wild type (wt) or empty vector control (mock) cells. Specific bands were detected similarly with M2 anti-FLAG antibody. Blotting with actin antibody was used as a loading control (bottom panels). (B) Migration analyses using Matrigel chambers. Parental wild type (wt), empty vector control (mock), and hLib-expressing cells (hLib) were plated on top of Matrigel-coated 8-μm filters. After 22 h, cells migrating through the filter were stained, visualized, and counted. (C) Graphical representation of average number of migration through Matrigel at 22 h. Results are means ± SEM from three independent experiments.

U87MG and H4 cells (Figs. 2B and C). These results demonstrate that Lib appears to be a LRR membrane protein that is involved in cell–ECM interactions important for glial migration.

Lib binds to extracellular matrix

Blot overlay assays were used to assess Lib binding to Matrigel and ECM macromolecules using affinity-purified extracellular region (aa 1–529) of hLib protein (Fig. 3A). Lib bound to fibronectin preferentially relative to Matrigel, collagen type IV or laminin, with minimal to no binding to aggrecan and BSA (Fig. 3B). Decreased dose of blotted macromolecules resulted in reduction of signal intensities.

Discussion

In the present study, we evaluated hLib mRNA expression in AD brains in comparison with age-matched non-AD brains. Human Lib mRNA was detected in activated astrocytes around senile plaques in AD and in these areas the signals for hLib mRNA in neurons were not observed. Similar to results from in vitro studies on rLib in rat astrocytes [6], hLib is also a distinctly inducible gene in human astrocytes in vivo, because signals for hLib mRNA were detected in reactive astrocytes in AD brain, but not in quiescent astrocytes in non-AD brain nor in lesion-free areas of AD brains. In contrast, neurons express hLib mRNA in non-AD brains and in lesion-free areas of AD

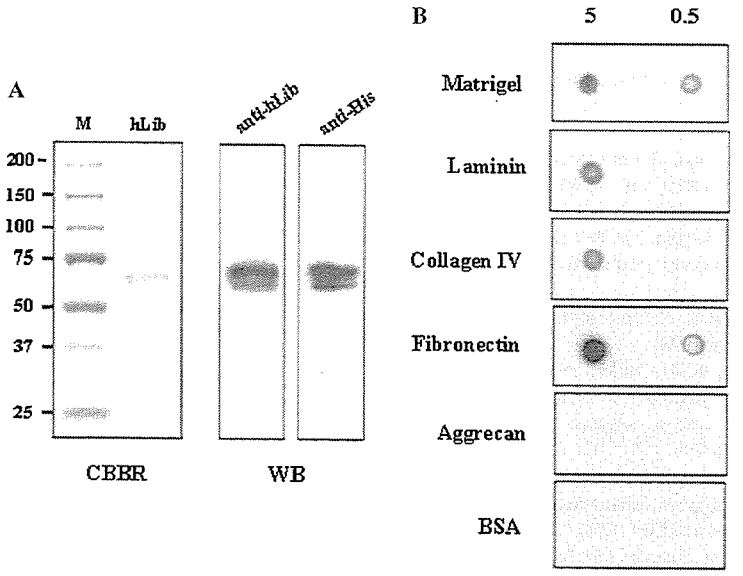

Fig. 3. Binding of hLib to ECM molecules. (A) Recombinant extracellular region of hLib was affinity purified from cultured supernatants of infected sf9 cells, followed by electrophoresis, and staining with CBBR250 (CBBR, left panel) (M, molecular size marker) or Western blotting with anti-hLib antibody (WB, right panel). (B) Matrigel, laminin, collagen type IV, fibronectin, aggrecan, and BSA were immobilized on PVDF membrane at 5 μg and 0.5 μg/spot. The PVDF membrane was then incubated with recombinant hLib, excessively washed, and immuno-detected using anti-hLib antibody.

brains. These results suggest that hLib expression may be required for maintenance of homeostasis in neuronal activities, although it is not clear whether loss of hLib mRNA in neurons of AD brains is caused by cellular death or loss of homeostasis in diseased neurons. It is also possible that Lib may play different roles in astrocytes and neurons, because some LRR proteins are involved in the regulation of neurite guidance and synapse formation [15–17].

Based on the presence of the LRR motif, Lib has been thought to play a role in specific cell–cell and/or cell–matrix interactions in astrocytes. The finding, that hLib mRNA is transcriptionally induced in activated astrocytes of AD brains, prompted us to evaluate the possibility that hLib may participate in the accumulation of astrocytes around senile plaques in cell–matrix interactions. The current data show that glial cells expressing hLib display accelerated migration through Matrigel, a reconstituted ECM. This effect on cellular motility is consistent with an other study showing reduction of cellular migration after suppressing hLib expression in a tumor cell line [18]. In addition, hLib protein demonstrates binding to some ECM constituents with some preferentiality, similar to other LRR proteins [19–21]. These results suggest that Lib may contribute to the regulation of cell–matrix adhesion interactions with respect to astrocyte recruitment around senile plaques.

In our previous study, ADAMTS-4, an ECM-degrading enzyme, was screened out from the same Aβ-treated astrocyte cDNA library [22]. Other studies have demonstrated that matrix metalloprotease (MMP) activities responsible for degradation of ECM are higher in brains from AD patients than in controls, and that these ECM degradation enzymes are derived from astrocytes [23,24]. To investigate the possibility that these reported MMP (MMP-2, MMP-3, and MMP-9) activities were transcriptionally up-regulated in hLib-expressing glial cells, their mRNA expression levels were evaluated by reverse transcriptase PCR (RT-PCR). However, they were not increased in hLib-transfected cells compared to parental or control mock cells in both U87MG and H4 cells (data not shown).

Astrocyte recruitment toward lesions is thought to be dependent on chemotactic molecules, such as MCP-1, originated from the core of senile plaques in lesions [25], accompanied with recognition of, adhesion to, and reducing integrity of ECM. Lib appears to participate in these steps by specific protein–protein and/or matrix interactions. Further investigation into Lib molecular mechanisms may provide additional insight into astroglial motility around lesions, suggesting novel therapeutic strategies.

Acknowledgments

We greatly appreciate Seiji Takahara and Hidetoshi Tsuzaki for technical support and advice, and Yasuhide Hirota for helpful discussion and encouragement.

References

[1] C.J. Pike, B.J. Cummings, C.W. Cotman, Early association of reactive astrocytes with senile plaques in Alzheimer's disease, Exp. Neurol. 132 (1995) 172–179.

[2] E.G. McGeer, P.L. McGeer, The inflammatory response system of brain: implications for therapy of Alzheimer and other neurodegenerative diseases, Brain Res. 21 (1995) 195–218.

[3] R.E. Mrak, J.G. Sheng, W.S. Griffin, Glial cytokines in Alzheimer's disease: review and pathogenic implications, Hum. Pathol. 26 (1995) 816–823.

[4] D.W. Dickson, The pathogenesis of senile plaques, J. Neuropathol. Exp. Neurol. 56 (1997) 321–339.

[5] M. Johnstone, A.J. Gearing, K.M. Miller, A central role for astrocytes in the inflammatory response to beta-amyloid; chemokines, cytokines and reactive oxygen species are produced, J. Neuroimmunol. 93 (1999) 182–193.

[6] K. Satoh, M. Hata, H. Yokota, A novel member of the leucine-rich repeat superfamily induced in rat astrocytes by beta-amyloid, Biochem. Biophys. Res. Commun. 290 (2002) 756–762.

[7] B. Kobe, J. Deisenhofer, The leucine-rich repeat: a versatile binding motif, Trends Biochem. Sci. 19 (1994) 415–421.

[8] S.G. Buchanan, N.J. Gay, Structural and functional diversity in the leucine-rich repeat family of proteins, Prog. Biophys. Mol. Biol. 65 (1996) 1–44.

[9] B. Kobe, A.V. Kajava, The leucine-rich repeat as a protein recognition motif, Curr. Opin. Struct. Biol. 11 (2001) 725–732.

[10] K. Satoh, M. Hata, H. Yokota, High Lib mRNA expression in breast carcinomas, DNA Res. 11 (2004) 199–203.

[11] Z.S. Khachaturian, Diagnosis of Alzheimer's disease, Arch. Neurol. 42 (1985) 1097–1105.

[12] S.S. Mirra, A. Heyman, D. McKeel, S.M. Sumi, B.J. Crain, L.M. Brownlee, F.S. Vogel, J.P. Hughes, G. van Belle, L. Berg, The Consortium to Establish a Registry for Alzheimer's Disease (CERAD). Part II. Standardization of the neuropathologic assessment of Alzheimer's disease, Neurology 41 (1991) 479–486.

[13] T. Yamada, Y. Tsujioka, J. Taguchi, M. Takahashi, Y. Tsuboi, T. Shimomura, White matter astrocytes produce hepatocyte growth factor activator inhibitor in human brain tissues, Exp. Neurol. 153 (1998) 60–64.

[14] V.M. Paralkar, B.S. Weeks, Y.M. Yu, H.K. Kleinman, A.H. Reddi, Recombinant human bone morphogenetic protein 2B stimulates PC12 cell differentiation: potentiation and binding to type IV collagen, J. Cell Biol. 119 (1992) 1721–1728.

[15] E. Shishido, M. Takeichi, A. Nose, *Drosophila* synapse formation: regulation by transmembrane protein with Leu-rich repeats, CAPRICIOUS, Science 280 (1998) 2118–2121.

[16] J.A. Howitt, N.J. Clout, E. Hohenester, Binding site for Robo receptors revealed by dissection of the leucine-rich repeat region of Slit, EMBO J. 23 (2004) 4406–4412.

[17] J. Kuja-Panula, M. Kiiltomaki, T. Yamashiro, A. Rouhiainen, H. Rauvala, AMIGO, a transmembrane protein implicated in axon tract development, defines a novel protein family with leucine-rich repeats, J. Cell Biol. 160 (2003) 963–973.

[18] P.A. Reynolds, G.A. Smolen, R.E. Palmer, D. Sgroi, V. Yajnik, W.L. Gerald, D.A. Haber, Identification of a DNA-binding site and transcriptional target for the EWS-WT1(+KTS) oncoprotein, Genes Dev. 17 (2003) 2094–2107.

[19] R.V. Iozzo, The biology of the small leucine-rich proteoglycans. Functional network of interactive proteins, J. Biol. Chem. 274 (1999) 18843–18846.

[20] K. Saito, T. Tanaka, H. Kanda, Y. Ebisuno, D. Izawa, S. Kawamoto, K. Okubo, M. Miyasaka, Gene expression profiling of mucosal addressin cell adhesion molecule-1+ high endothelial venule cells (HEV) and identification of a leucine-rich HEV glycoprotein as a HEV marker, J. Immunol. 168 (2002) 1050–1059.

[21] A.N. Malhas, R.A. Abuknesha, R.G. Price, Interaction of the leucine-rich repeats of polycystin-1 with extracellular matrix proteins: possible role in cell proliferation, J. Am. Soc. Nephrol. 13 (2002) 19–26.

[22] K. Satoh, N. Suzuki, H. Yokota, ADAMTS-4 (a disintegrin and metalloproteinase with thrombospondin motifs) is transcriptionally induced in beta-amyloid treated rat astrocytes, Neurosci. Lett. 289 (2000) 177–180.

[23] A. Lukes, S. Mun-Bryce, M. Lukes, G.A. Rosenberg, Extracellular matrix degradation by metalloproteinases and central nervous system diseases, Mol. Neurobiol. 19 (1999) 267–284.

[24] S. Deb, P.E. Gottschall, Increased production of matrix metalloproteinases in enriched astrocyte and mixed hippocampal cultures treated with beta-amyloid peptides, J. Neurochem. 66 (1996) 1641–1647.

[25] T. Wyss-Coray, J.D. Loike, T.C. Brionne, E. Lu, R. Anankov, F. Yan, S.C. Silverstein, J. Husemann, Adult mouse astrocytes degrade amyloid-beta in vitro and in situ, Nat. Med. 9 (2003) 453–457.

Cellular and Molecular Neurobiology, Vol. 25, No. 5, August 2005 (©2005)
DOI: 10.1007/s10571-005-4956-5

Short Communication

Cyclosporin A Aggravates Electroshock-Induced Convulsions in Mice with a Transient Middle Cerebral Artery Occlusion

Atsushi Yamauchi,[1] Hideki Shuto,[1] Shinya Dohgu,[1] Yoshitsugu Nakano,[1] Takashi Egawa,[1] and Yasufumi Kataoka[1,2]

Received January 11, 2005; accepted February 18, 2005

SUMMARY

1. To test whether an ischemic insult increases the susceptibility to cyclosporine A (CsA)-induced neurotoxicity, we examined the effect of CsA on the minimal electroshock-induced convulsions in mice treated with a transient middle cerebral artery occlusion (MCAO) for a short period (2 h).

2. This MCAO produced small to mid-sized infarcted regions in the cerebral hemisphere with increasing post-operative days. In MCAO mice, CsA (30 mg/kg, i.p.) elevated the incidence of minimal electroshock-induced convulsions to 90–100% over that in sham mice (20–30%) at 1–7 days but not 14 days post-surgery.

3. In light of these findings, the possibility that CsA increases the risk of convulsions in patients with cerebral infarction and/or at an early stage following focal cerebral ischemia would have to be considered.

KEY WORDS: cyclosporin A; electroshock-induced convulsions; middle cerebral artery occlusion; blood-brain barrier; mice.

INTRODUCTION

Cyclosporin A (CsA), an immunosuppressant, is widely used to prevent allograft rejection in solid organ transplantation and to treat various autoimmune diseases. CsA induces adverse events including renal, cardiovascular and gastrointestinal disorders. Neurological complications occur with a relatively high frequency (20–40%) (Gijitenbeek *et al.*, 1999; U. S. Group, 1994). The delivery of CsA into the brain is

[1] Department of Pharmaceutical Care and Health Sciences, Faculty of Pharmaceutical Sciences, Fukuoka University, 8-19-1 Nanakuma, Jonan-ku, Fukuoka 814-0180, Japan.
[2] To whom correspondence should be addressed; e-mail: ykataoka@cis.fukuoka-u.ac.jp.

restricted by P-glycoprotein, a multi-drug efflux pump, and the tight junctions of brain capillary endothelial cells. CsA inhibited the function and expression of P-glycoprotein (Kochi *et al.*, 1999) and increased the permeability of brain endothelial cells (Dohgu *et al.*, 2000), suggesting that CsA could pass through the blood-brain barrier (BBB) due to the impaired function. In the present study, to test whether CsA induces neurotoxicity by passing through the damaged BBB and/or the reconstituted BBB with an incomplete function after an ischemic insult, we examined the effect of CsA on minimal electroshock-induced convulsions in mice treated with a transient middle cerebral artery occlusion (MCAO) for a short period (2 h).

MATERIALS AND METHODS

Male ddY mice weighing 25–35 g (Kyudo, Kumamoto, Japan) were housed in a room at a temperature of 22 ± 2°C under a 12-h light/dark schedule (lights on at 7:00 hours) and given water and food ad libitum. All the procedures involving experimental animals adhered to the law (No. 105) and notification (No. 6) of the Japanese Government, and were approved by the Laboratory Animal Care and Use Committee of Fukuoka University.

The pharmaceutical formulation of CsA (Sandimmun® injection, 250 mg/5 mL/ampule, Novartis Pharma, Tokyo, Japan) was used after a dilution with saline. The vehicle solution for CsA consisted of 13% polyoxyethylene castor oil (Cremophor EL®, Sigma, St. Louis, MO, USA), 7% ethanol, and 80% saline (the same mixture as the vehicle for Sandimmun® injection). A reagent for histological examination, 2,3,5-triphenyltetrazolium chloride (TTC), was purchased from Sigma.

Anesthesia was induced by 2% halothane (Flosen, Takeda, Osaka, Japan) and maintained with 1% halothane. Focal cerebral ischemia was induced by occlusion of the middle cerebral artery using the intraluminal filament technique (Mishima *et al.*, 2003). After a midline neck incision, the left common and external carotid arteries were isolated and ligated. An 8-0 nylon monofilament (Ethilon, Johinson & Johinson, Tokyo, Japan) coated with silicon resin (Xantopren, Heleus Dental Material, Osaka, Japan) was introduced through a small incision into the common carotid artery and was advanced to a position 9 mm distal from the carotid bifurcation for occlusion of the middle cerebral artery. Two hours after MCAO, animals were re-anesthetized with halothane, and reperfusion was established by withdrawal of the filament. The sham-operated mice were subjected to the procedure mentioned above without MCAO. At the end of the experiment, mice were decapitated under anesthesia with pentobarbital Na (40 mg/kg, i.p., Nembutal, Dainippon, Osaka, Japan) and brains were removed. Coronal sections were cut 2-mm thick and incubated in physiological saline containing 2% TTC at 37°C for 15 min for histological examination of the MCAO-induced brain damage.

Effect of CsA or vehicle on the minimal electroshock-induced convulsions was examined at 1, 3, 7 and 14 days after the sham-operation or MCAO. CsA (10 and 30 mg/kg) or vehicle was administered i.p. in a volume of 0.1 mL/10 g body weight. Sixty minutes after the injection, each mouse was subjected to the minimal electroshock (10 mA, at a frequency of 60 Hz, applied for 0.2 s) using

external corneal electrodes connected to an electroshock convulsive stimulator unit (MK-800, Muromachi Kikai, Tokyo, Japan) and placed individually in an acrylic cage (18 × 28 × 34 cm). The observations were made during a 2-min period with a camcorder (VL-DC1, Sharp, Tokyo, Japan) and stored on digital video tape. The durations of clonic and tonic-clonic convulsions were measured with a video player by two observers blinded to the pretreatment with CsA or vehicle. The minimal electroshock-induced convulsions were defined as positive when they lasted for more than 2 s. Only one of 12 normal mice showed convulsions for 1 s.

Statistical analysis was performed using Fisher's exact probability test. A value of $P < 0.05$ was considered significant.

RESULTS

Histological observations with TTC staining indicated that MCAO for 2 h produced a small infarcted region in the caudate putamen of the cerebral hemisphere with a relatively mild insult (an irregular pallor) at 1 day after the operation (Fig. 1). The size and intensity of infarction gradually increased in the cuadate putamen and cerebral cotex at 3–7 days, reaching a maximum at 14 days. Minimal electroshock did not induce convulsions in sham mice treated with vehicle. When CsA (10 or 30 mg/kg) was given, convulsions were induced by electroshock in 20–30% of sham mice at 1–14 days post-surgery (Fig. 2A). In MCAO mice treated with vehicle, electroshock-induced convulsion was observed in 1 of 8 mice at 1 day, but not at 3–14 days post-surgery (Fig. 2B). In MCAO mice, CsA (10 mg/kg) moderately increased the incidence of convulsions to 67% over the level in sham mice (20–30%) at 1 day but not at 3–14 days after operation (Fig. 2). CsA (30 mg/kg) markedly increased the incidence of convulsions to 90–100% at 1–7 days, but this increase was not observed at 14 days after the operation in MCAO mice (Fig. 2B).

DISCUSSION

Treatment with MCAO is employed to make an animal model of transient focal cerebral ischemia (Brown *et al.*, 1995; Sydserff *et al.*, 2002). In the present study, a short (2 h) MCAO produced small to mid-sized infarcted regions with increasing post-operative days in the caudate putamen and cerebral cortex, when compared with the usual MCAO method (4 h) (Mishima *et al.*, 2003) (Fig. 1).

A high dose of CsA (30 mg/kg) markedly aggravated the electroshock-induced convulsions in MCAO mice. This action appeared at an early stage (1–7 days) but not late stage (14 days) post-MCAO. An ischemic event has been known to cause disruption of the BBB (Cipolla *et al.*, 2004). Nishigaya *et al.* demonstrated using an immunohistological staining of endothelial barrier antigen that impairment and restoration of the brain endothelial barrier occurred in the post-ischemic period of 1–7 days and 14–28 days, respectively, in rats with MCAO for 2 h. Taken together with this evidence, the present findings suggest that CsA probably penetrates the brain through the impaired BBB at an early stage following ischemic insults and consequently has an adverse central action. The reconstituted BBB at a late-stage

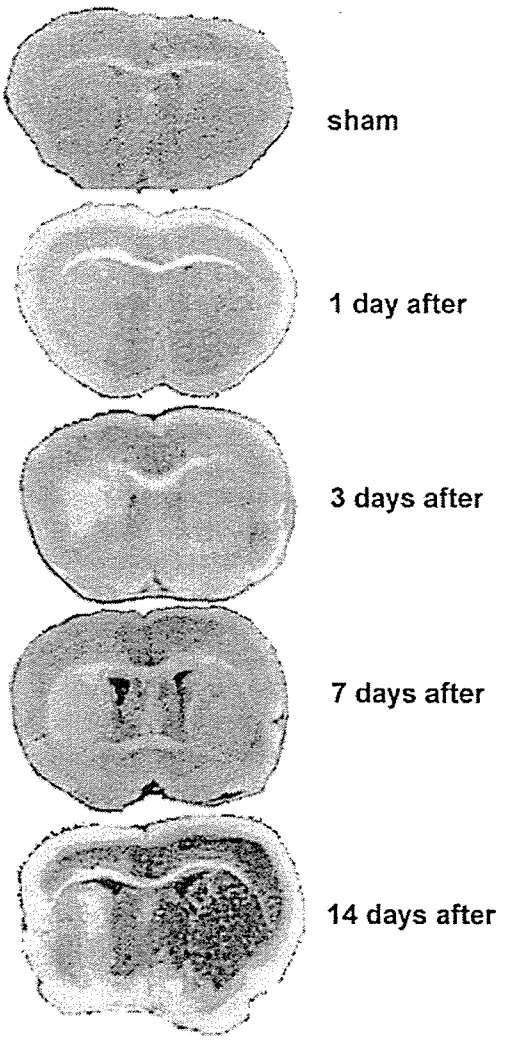

Fig. 1. Representative photographs showing coronal sections of the caudate putamen and cerebral cortex stained with 2% 2,3,5-triphenyltetrazolium chloride at 1, 3, 7 and 14 days after a transient middle cerebral artery occlusion for 2 h and at 7 days after sham operation (Sham).

post-MCAO may limit the delivery of CsA. Our previous findings *in vitro* demonstrated that CsA impairs brain endothelial barrier function by accelerating NO production in brain endothelial and astroglial cells (Ikesue *et al.*, 2000; Dohgu *et al.*, 2000; Yamauchi *et al.*, 2005). This action of CsA may be effective against the damaged BBB and/or the reconstituted BBB with an incomplete function at an early stage following the pathological insult. CsA is known to induce convulsions as a result of an

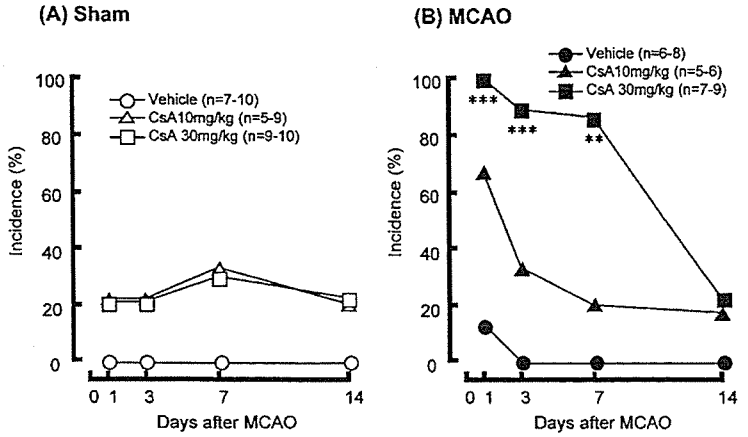

Fig. 2. Effect of cyclosporin A (CsA) on minimal electroshock-induced convulsions in sham-operated mice (Sham) (A) and in mice with a transient middle cerebral artery occlusion for 2 h (MCAO) (B). Values are expressed as the incidence (%) of convulsions in mice injected with vehicle or CsA 1 h before the test. The number of mice used in each treatment is indicated in parentheses. $^{**}P < 0.01$ and $^{***}P < 0.001$; significant difference from each corresponding group treated with vehicle.

interaction between NO and the γ-aminobutyric acid system in the hippocampus (Shuto *et al.*, 1999; Fujisaki *et al.*, 2002). This may be interpreted as a possible mechanism for the adverse central action of CsA after penetration of the brain. The possibility that MCAO influences these neuronal systems and increases the susceptibility to the deleterious effect of CsA on convulsions could not be excluded.

There is experimental evidence that CsA at low doses produces neuroprotective effects when given 30 min before or several minutes to 3 h after brain ischemia (Kuroda *et al.*, 1999; Yoshimoto *et al.*, 1999). In these studies, CsA prevented neuronal cell death including necrosis and apoptosis and decreased the infarct volumes in the brain. The different dosing schedule and doses of CsA are probably responsible for the discrepancy in the results.

In light of these findings, the possibility that CsA increases the risk of convulsions in patients with cerebral infarction and/or at an early stage following focal cerebral ischemia would have to be considered.

ACKNOWLEDGMENTS

This work was supported, in part, by Grants-in-Aid for Scientific Research ((B)(2) 14370789) and ((C)(2) 15590475) from JSPS, Japan, by a Grant-in-Aid for Exploratory Research (16659138) from MEXT, Japan, by funds (No.: 031001) from the Central Research Institute of Fukuoka University and by MEXT. HAITEKU (2000–2004).

REFERENCES

Brown, C. M., Calder, C., Linton, C., Small, C., Kenny, B. A., Spedding, M., and Patmore, L. (1995). Neuroprotective properties of lifarizine compared with those of other agents in a mouse model of focal cerebral ischaemia. *Br. J. Pharmacol.* **115:**1425–1432.

Cipolla, M. J., Crete, R., Vitullo, L., and Rix, R. D. (2004). Transcellular transport as a mechanism of blood-brain barrier disruption during stroke. *Front. Biosci.* **9:**777–785.

Dohgu, S., Kataoka, Y., Ikesue, H., Naito, M., Tsuruo, T., Oishi, R., and Sawada, Y. (2000). Involvement of glial cells in cyclosporine-increased permeability of brain endothelial cells. *Cell. Mol. Neurobiol.* **20:**781–786.

Fujisaki, Y., Yamauchi, A., Dohgu, S., Sunada, K., Yamaguchi, C., Oishi, R., and Kataoka, Y. (2002). Cyclosporine A-increased nitric oxide production in the rat dorsal hippocampus mediates convulsions. *Life Sci.* **72:**549–556.

Gijitenbeek, J. M. M., Van den Bert, M. J., and Vecht, Ch. J. (1999). Cyclosporine neurotoxicity: A review. *J. Neurol.* **246:**339–346.

Ikesue, H., Kataoka, Y., Kawachi, R., Dohgu, S., Shuto, H., and Oishi, R. (2000). Cyclosporine enhances α1-adrenoreceptor-mediated nitric oxide production in C6 glioma cells. *Eur. J. Pharmacol.* **407:**221–226.

Kochi, S., Takanaga, H., Matsuo, H., Naito, M., Tsuruo, T., and Sawada, Y. (1999). Effect of cyclosporine A or tacrolimus on the function of blood-brain barrier cells. *Eur. J. Pharmacol.* **372:**287–295.

Kuroda, S., Janelidze, S., and Siesjo, B. K. (1999). The immunosuppressants cyclosporin A and FK506 equally ameliorate brain damage due to 30-min middle cerebral artery occlusion in hyperglycemic rats. *Brain Res.* **835:**148–153.

Mishima, K., Tanaka, T., Pu, F., Egashira, N., Iwasaki, K., Hidaka, R., Matsunaga, K., Takata, J., Karube, Y., and Fujiwara, M. (2003). Vitamin E isoforms alpha-tocotrienol and gamma-tocopherol prevent cerebral infarction in mice. *Neurosci. Lett.* **337:**56–60.

Nishigaya, K., Yagi, S., Sato, T., Kanemaru, K., and Nukui, H. (2000). Impairment and restoration of the endothelial blood-brain barrier in the rat cerebral infarction model assessed by expression of endothelial barrier antigen immunoreactivity. *Acta Neuropathol.* **99:**231–237.

Shuto, H., Kataoka, Y., Fujisaki, K., Nakao, T., Sueyasu, M., Miura, I., Watanabe, Y., Fujiwara, M., and Oishi, R. (1999). Inhibition of GABA system involved in cyclosporine-induced convulsions. *Life Sci.* **65:**879–887.

Sydserff, S. G., Borelli, A. R., Green, A. R., and Cross, A. J. (2002). Effect of NXY-059 on infarct volume after transient of permanent middle cerebral artery occlusion in the rat; studies on dose, plasma concentration and therapeutic time window. *Br. J. Pharmacol.* **135:**103–112.

The U.S. Multicenter FK506 Liver Study Group (1994). A comparison of tacrolims (FK 506) and cyclosporine for immunosuppression in liver transplantation. *N. Engl. J. Med.* **331:**1110–1115.

Yamauchi, A., Dohgu, S., Naito, M., Tsuruo, T., Sawada, Y., Kai, M., and Kataoka, Y. (2005). Nitric oxide lowers the function of tight junction and P-glycoprotein at the blood-brain barrier. *Cell. Mol. Neurobiol.* in press.

Yoshimoto, T., and Siesjo, B. K. (1999). Posttreatment with the immunosuppressant cyclosporin A in transient focal ischemia. *Brain Res.* **839:**283–291.

Science Express

Reciprocal Interference Between Specific CJD and Scrapie Agents in Neural Cell Cultures

Noriuki Nishida, Shigeru Katamine, Laura Manuelidis

21 October 2005, Volume 310, pp. 493-496

Reciprocal Interference Between Specific CJD and Scrapie Agents in Neural Cell Cultures

Noriuki Nishida,[1,2] Shigeru Katamine,[3] Laura Manuelidis[1]*

Infection of mice with an attenuated Creutzfeldt-Jakob disease agent (SY-CJD) interferes with superinfection by a more virulent human-derived CJD agent (FU-CJD) and does not require pathological prion protein (PrPres). Using a rapid coculture system, we found that a neural cell line free of immune system cells similarly supported substantial CJD agent interference without PrPres. In addition, SY-CJD prevented superinfection by sheep-derived Chandler (Ch) and 22L scrapie agents. However, only 22L and not Ch prevented FU-CJD infection, even though both scrapie strains provoked abundant PrPres. This relationship between particular strains of sheep- and human-derived agents is likely to affect their prevalence and epidemic spread.

In transmissible spongiform encephalopathies (TSEs) such as human CJD, sheep scrapie, and bovine spongiform encephalopathy (BSE), B and T cell adaptive immune responses to a foreign infectious agent have not been detected (*1*). Nonetheless, an attenuated CJD agent, designated SY, was able to prevent superinfection by the more virulent and rapidly lethal FU-CJD agent (*2*). These experiments exploited two human CJD agents that, when passaged in mice, were readily distinguished by profound differences in the incubation time to disease and the distribution of brain lesions. The attenuated "slow" SY produced only small medial thalamic lesions typical of sporadic CJD in mice, whereas the virulent "fast" FU strain, isolated only in Japan, caused widespread severe lesions with many amyloid deposits (Table 1). Clear protective effects of SY-CJD against superinfection by FU-CJD were demonstrable with both intracerebral and peripheral challenges, and SY-protected mice could live free of disease for >600 days, a typical mouse life span (*3*, *4*). By comparison, there was minimal interference between scrapie strains 22C and 22A (*5*). This raised the possibility that protective effects might be restricted to particular strains of CJD or to unusual agent strain combinations. We sought ways to evaluate interference between different combinations of TSE agents, and to determine whether apparently unrelated agents—such as those propagated from human CJD and from sheep scrapie cases—could be antagonistic.

Mice can respond to CJD agents through a variety of myeloid cell and innate defense mechanisms (*6*–*8*). Thus, it was relevant to determine whether different agent strains could prevent superinfection in simplified cell cultures that lack B, T, and myeloid cells. Neural cells, which can be susceptible to TSE agents, would be incapable of producing many of the myeloid cell cytokines that can participate in strain interference in vivo. If interference could be demonstrated in neural cells, it would show that more universal cellular pathways are sufficient for protection. These culture models also might be used to identify crucial, and possibly novel, molecular pathways of innate immunity to TSE agents.

We developed a rapid, simple, and flexible test of interference in GT1-7 cells (hereafter called GT cells), a murine hypothalamic cell line. We previously found that these cells support the replication of a variety of mouse-passaged CJD and scrapie agents (Table 1) (*9*, *10*). A neomycin-resistant plasmid was introduced into the target GT cells (GTneo) to allow their selection by G418 antibiotic treatment (*11*) (Fig. 1). Infected GT challenge cells were killed by adding G418 to cocultures, and the pure GTneo target cells were then passaged and assayed for PrPres, a surrogate marker for infection in GT cells. Although PrPres does not quantitatively correlate with infectious

[1]Yale Medical School, New Haven, CT 06510, USA. [2]Center for Emerging Infectious Diseases, Gifu University, Yanagido 1-1, Gifu 501-1193, Japan. [3]Department of Molecular Microbiology and Immunology, Nagasaki University Graduate School of Medicine, 1-12-4 Sakamoto, Nagasaki 852-8523, Japan.

*To whom correspondence should be addressed. E-mail: laura.manuelidis@yale.edu

Table 1. Cell lines and TSE agents for testing interference. Agents, their source, and the number of cell passages after infection at the time of challenge are shown. By convention, TSE agent names identify the natural host. Thus, scrapie agents are derived from sheep, CJD agents from humans, CWD agents from cervids, and BSE agents from cows. Hence, the terms mouse scrapie and PrP^{Sc} (i.e., PrPres in mice infected with scrapie) indicate infection with sheep-derived agents. The UK Chandler (Ch) "drowsy" strain [equivalent to Rocky Mountain Laboratory (RML) scrapie], from a goat with experimental scrapie, is distinct from 22L scrapie (typical scratching scrapie in sheep from brain pool SSBP1). These scrapie strains are clearly different from CJD and BSE agents propagated in mice (i.e., their separate identities are not made homogeneous by the murine host). CJD encompasses all subsets of human TSE infectious agents except kuru, including those isolated from patients with PrP mutations such as PrP 102L of Gerstmann-Sträussler-Sheinker disease (GSS). SY-CJD causes circumscribed thalamic lesions only after ≥350 days in mice, and it is representative of sporadic CJD agents in the Western hemisphere, including agents isolated from GSS patients (*23*). No CJD agent similar to the representative Japanese fast FU-CJD agent ("CJD-Fukuoka-1") that induces widespread PrP amyloid deposits and severe demyelination has ever been isolated outside of Japan. Because FU-CJD and the Ch and 22L scrapie strains all cause widespread brain pathology, interference between these strains cannot be assessed in mice.

Cell line	Agent strain	Origin	Passages
GT (GT1-7)	—	—	—
SY+GT	SY	CJD sporadic: USA	≥106
FU+GT	FU	CJD (GSS 102L): Japan	≥110
Ch+GT	Ch	"Drowsy" scrapie: UK	≥50
22L+GT	22L	"Scratching" scrapie: UK	≥50
GTneo	Mock	—	≥15
SY+GTneo	SY	CJD sporadic: USA	≥110
Ch+GTneo	Ch	"Drowsy" scrapie: UK	≥15
22L+GTneo	22L	"Scratching" scrapie: UK	≥15

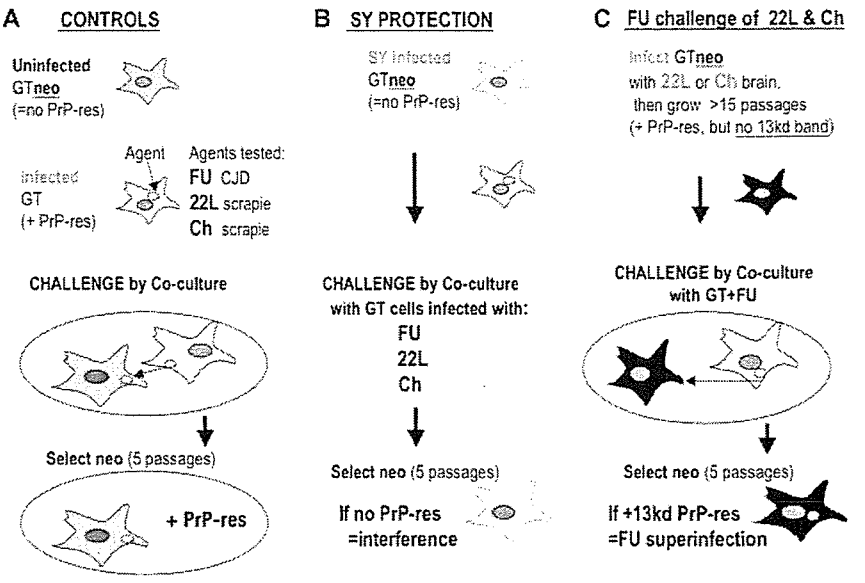

Fig. 1. In vitro interference strategy: Coculture challenges of (A) uninfected control cells, (B) SY-infected cells, and (C) scrapie-infected cells. Target GTneo cells were challenged with mock GT or infected GT cells by coculture for 2 days. GT challenge cells were then killed by G418 treatment, and resistant GTneo cells were analyzed for PrPres (*11*). For FU challenges, GTneo cells were newly infected with 22L or Ch scrapie brain homogenates and passaged >15 times before coculture.

titers, and may not be detectable in all infectious samples [e.g., (*1*, *4*, *12*, *13*)], its presence does indicate infection in GT cells (*10*).

GTneo target cells were exposed to uninfected brain tissue or to equal numbers of uninfected donor cells (i.e., mock-infected as in Fig. 1A). Such control GTneo cells should fail to produce PrPres. In contrast, mock-infected GTneo cells challenged with infected GT cells should become persistently infected and display PrPres long after the GT cells are removed by G418 treatment. Challenges of GTneo cells by GT cells infected with the agents 22L scrapie (GT+22L), Ch scrapie (GT+Ch), or FU-CJD (GT+FU) were rapidly effective (Fig. 2A). A large amount of PrPres was produced by all the control target cells after challenge with infected GT cells, but no PrPres was present after exposure to uninfected brain tissue (in this and in three or more repeat experiments per condition). Further in vitro passages of these GTneo target cells showed stable production of PrPres, indicating persistent infection by each of the challenge agents. Some TSE agents have been associated with variant PrPres band patterns (*14*). The three major PrPres bands were the same in all infected cells. However, an extra, highly reproducible, 13-kD band of PrPres was seen only in FU-infected cells. Antibodies identified this as a C-terminal PrPres fragment (Fig. 2A, C-13). Because this band was not present with any of the other agents, we could use it to specifically diagnose FU superinfection. Moreover, with all challenge agents, rapid infection with de novo production of large amounts of PrPres was apparent by 25 days in culture, whereas intracerebral inoculation with FU homogenates takes more than 90 days to induce brain PrPres (*8*).

In parallel with these controls, we tested whether SY could interfere with FU superinfection in culture as it does in mice, and we also tested whether SY infection could reduce susceptibility to presumably unrelated scrapie agents (Fig. 1B). The neomycin plasmid was added to PrPres-negative but persistently infected SY cells (as verified by repeated bioassays) (*10*, *11*). The lack of PrPres in SY-infected target cells greatly simplified the interference assay. After challenge, a continued lack of PrPres would indicate that covert SY infection protected cells from superinfection. In all these experiments, the number of infectious particles in challenge cells was higher than in target cells by a factor of ≥10,000 (*11*). No PrPres was detected in the GTneo+SY cells challenged with 22L cells (SY/22L lane, Fig. 2B). Thus, SY infection interfered with 22L superinfection. G418 selection also visibly removed all of the abundant PrPres of challenge cells. Persistent SY infection additionally interfered with GT+Ch scrapie agent and GT+FU CJD agent challenges. Only a barely detectable smear of signal was seen in the PrPres gel region (Fig. 2B). Moreover, the 13-kD PrPres band elicited by FU infection was never detectable in the FU-challenged SY cells, and the lack of any distinguishing strain-specific PrPres patterns for the other three common major PrPres bands made it impossible to determine whether the ± signal was due to low levels of the challenge strain. Two repeat experiments reconfirmed that SY interfered with superinfection by 22L, Ch, and FU agents (Table 2). Although the PrPres results do not permit us to conclude that there was complete prevention of superinfection, the interference of SY against 22L, Ch, and FU agents in vitro was manifest, and in marked contrast to the results with unprotected cells.

Because the 13-kD PrPres band was seen only after FU infection (Fig. 2A), it was possible to test whether scrapie agents could protect against the FU-CJD agent (Fig. 1C). We established new persistent infections of GTneo cells by standard application of infected brain homogenates (*9*, *10*), and verified that these newly infected GTneo cells continued to produce substantial amounts of

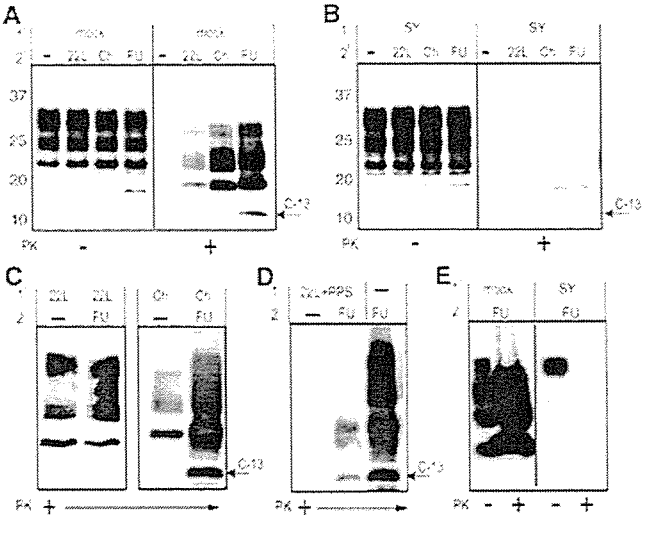

Fig. 2. Immunoblots of control and infected target cells. (A) Challenge of mock-infected and (B) SY-CJD–infected GTneo target cells by coculture with uninfected GT cells (–) or with infected GT+22L, GT+Ch, and GT+FU cells. Primary agent (1°) and challenge agent (2°) are indicated with total PrP compared to PrPres after limited proteinase K (PK) digestion. No PrPres is detectable in SY-infected cells, and the C-13 band is seen only in FU-infected cells. Markers (in kilodaltons) are at left. (C) PrPres after mock (–) and FU-CJD challenge (FU) of 22L scrapie GTneo cells (left) versus challenge of Ch scrapie GTneo cells (right). Mock controls (–) both show high levels of PrPres in scrapie-infected cells before FU challenge. After FU challenge of 22L cells, the pattern and amount of PrPres is unchanged, indicating no appreciable superinfection, and the C-13 band is undetectable. In contrast, massive superinfection by FU is apparent in Ch-infected cells, with markedly increased PrPres and a clear 13-kD band (C-13). (D) Superinfection of "cured" 22L cells treated with pentosan polysulfate (22L+PPS). PrPres is not detectable in the "cured" unchallenged cells (left lane) as compared with the original 22L-infected cells in (C). "Cured" cells challenged with FU became susceptible to FU superinfection and showed the C-13 FU diagnostic band (middle lane, arrow). The "cured" cells, however, showed less PrPres than did the parallel FU-challenged uninfected controls (right lane), possibly suggesting residual 22L scrapie agent. (E) Mock- and SY-infected target cells (minus neo plasmid or G418 selection) challenged with GT+FU cells separated by a 0.4μ filter. Mock cells became infected (positive for PrPres, left), whereas SY-infected cells were protected (right). C-13 is not seen in whole-cell lysates (*11*).

Table 2. Interference results in three replicate experiments. Symbols: +, strong PrPres signal (positive infection); –, no detectable PrPres; ±, barely detectable or questionable PrPres signal between 19 and 30 kD. C-13 is the FU diagnostic band. FU-CJD, 22L, and Ch scrapie infectious challenges were of greater magnitude than in previous in vivo studies (*11*).

Agent		PrPres		Interference
1° first	2° challenge	19 to 30 kD	C-13	
Mock	FU-CJD	+ / + / +	+ / + / +	No
Mock	22L scrapie	+ / + / +	– / – / –	No
Mock	Ch scrapie	+ / + / +	– / – / –	No
SY-CJD	Mock	– / – / –	– / – / –	—
SY-CJD	FU-CJD	± / – / –	– / – / –	Yes
SY-CJD	22L scrapie	– / ± / ±	– / – / –	Yes
SY-CJD	Ch scrapie	± / – / –	– / – / –	Yes
22L scrapie	FU-CJD	+ / + / +	– / – / –	Yes
Ch scrapie	FU-CJD	+ / + / +	+ / + / +	No

pathologic PrPres for >15 in vitro passages before challenging them with GT+FU cells. Both the 22L and Ch scrapie–infected GTneo cells, but not the parallel mock-infected cells, showed large amounts of the three major PrPres bands, but not the extra 13-kD band that was diagnostic for FU infection. These 22L and Ch scrapie–infected GTneo cells were then challenged with FU+GT cells that displayed the 13-kD band (as in Fig. 2A). A large increase in PrPres and/or the appearance of the extra 13-kD PrPres band in scrapie-infected GTneo cells would show that these particular scrapie agents failed to prevent superinfection by FU. Superinfection would also prove that high levels of PrPres are not protective.

The scrapie strains 22L and Ch displayed markedly different capacities for interfering with FU superinfection (Fig. 2C). Target 22L cells were protected against FU superinfection. The PrPres intensity and band patterns of 22L cells exposed to FU (22L/FU lane, Fig. 2C) were the same as in 22L controls (22L/– lane), and the lack of the FU-diagnostic 13-kD PrPres band further confirmed that only the initial 22L infection was present. The 13-kD PrPres band also did not appear with additional in vitro passages, indicating that FU was probably not covertly contaminating the target cells. These results were reproducible (Table 2).

In sharp contrast, Ch scrapie infection did not protect GTneo cells from FU superinfection. PrPres accumulation in these FU-challenged cells (Ch/FU lane, Fig. 2C) was considerably more intense than in mock cells (Ch/– lane), and consistent with the amount of pathologic PrPres that would be provoked by infection with both agents. Additionally, there was a strong 13-kD PrPres signal indicating FU superinfection (Fig. 2C and Table 2). Hence, enormous amounts of PrPres provoked by the Ch agent did not prevent massive superinfection by a second strain. Because in situ studies show that FU infects most GT cells (*10*), it is likely that a fair proportion of the Ch/FU cells were doubly infected. Brain tissue can also be doubly infected, and each agent breeds true despite cocultivation in that tissue for >200 days (*3*). In sum, two scrapie strains eliciting the same PrPres band pattern show markedly different susceptibilities to a CJD agent that provokes an extra PrPres band.

To further show that interference depended on persistent infection, we "cured" GT+22L neo cells by treating them with pentosan polysulfate (*11*) until PrPres was undetectable (Fig. 2D). We then challenged these "cured" 22L cultures and parallel mock controls with GT+FU as above. These "cured" cultures became susceptible to FU superinfection and showed the diagnostic FU 13-kD band (Fig. 2D), unlike the 22L-protected cells (Fig. 2C). This experiment also shows that the 22L agent, rather than some new cellular characteristic induced by neo plasmid/G418 selection, was the ultimate cause of interference.

Direct cell-to-cell contacts may aid agent transmission in vivo, as in the transfer of infectious agent from follicular dendritic cells to transiting white blood cells (*15*). We found that concentrated supernatants from both 22L- and FU-infected GT cells were less infectious than the remaining whole washed cells by a factor of ~1000, as measured by bioassay. We also prevented direct cell-to-cell contact with 0.4μ filters placed between challenge cells and GT+SY target (minus neoplasmid) cells. This would permit the transit of large viruses and aggregates but not whole cells. Equal numbers of healthy challenge and target cells were plated and exposed for 2 days, and the separated target cells were then passaged and analyzed (*11*). Target control cells required ≥8 in vitro passages to produce PrPres and did not always become positive, unlike the cocultures described above. However, despite this caveat, SY infection did interfere with FU superinfection as compared to more typical controls (Fig. 2E). Thus, SY infection rather than neo transformation and G418 selection was the primary cause of interference.

We have shown that infected neural cells in culture carry all the requisite features for

mounting a substantial TSE interference effect. No immune system cells were necessary for this protection, and stable interfering infections were reproducibly achieved without cloning. Interference did not depend on the presence or absence of abnormal PrP. Only persistent infection protected target cells from superinfection. Additionally, only particular agent-strain combinations showed positive interference, and these could not be predicted from cellular PrPres amounts or banding patterns. Moreover, despite continuous replication in cells with PrPres band patterns very different from those found in brain tissue, SY and FU CJD agents each breed true when reinoculated into mice, as does rodent-passaged scrapie reinoculated in sheep (*10*). The stability of the BSE agent also contrasts with the many different PrPres patterns seen in various affected species. Together, these results are not compatible with the common assumption that TSE strains are encoded by some unresolved type of PrPres folding (*16*, *17*). Indeed, there is still no conclusive evidence that any recombinant or amplified form of abnormal PrP can infect normal animals directly, reproduce meaningful levels of infectivity, or encode all the strain differences observed in mice infected with scrapie, CJD, and BSE agents.

Unlike heterogeneous aggregates of pathological PrP, infectious TSE particles have a discrete viral size of ~25 nm and 10^7 daltons (as assessed by field flow fractionation and high-pressure liquid chromatography, respectively) (*18*), and releasing their tightly bound nucleic acids destroys infectivity (*19*). Thus, some TSE agents such as SY may produce defective interfering particles, as found in many persistent viral as well as noncoding human viroid infections (*20*, *21*). Unlike pathologic host PrP, TSE agents can also provoke innate cellular defenses, including intracellular and diffusible factors that are not restricted to immune system cells (*7*, *8*), and such factors are likely to be involved in interference. Small interfering RNAs with extensive secondary structure may also be evoked by TSE agents, and these can provide even greater strain specificity (*22*). Notably, several small RNAs with extensive secondary structure have been identified in TSE-infected but not in normal brain tissue (*23*), and such motifs deserve further study in TSE culture models.

Cocultures were more efficient than mouse bioassays and can be useful for rapid assessment of agent purification and recovery (*24*). Additionally, they may provide a sensitive test for cells that are infected but show no PrPres (such as white blood cells), and they may be useful for evaluating a wide range of evolving TSE agents that have become important epidemiologically, such as those that cause BSE and chronic wasting disease (CWD). The resistance of cells infected with a prototypic sporadic CJD agent (SY) to two scrapie strains supports the suggestion that a commensal but rarely pathogenic TSE agent may help protect people against infection by sheep TSE strains in nature (*4*), and may explain why so few people have developed BSE-linked CJD (*25*). The clustering of sporadic CJD cases is also consistent with an environmental agent of low virulence (*26*).

References and Notes

1. L. Manuelidis, W. Fritch, Y. G. Xi, *Science* **277**, 94 (1997).
2. L. Manuelidis, *Proc. Natl. Acad. Sci. U.S.A.* **95**, 2520 (1998).
3. L. Manuelidis, Z. Y. Lu, *Neurosci. Lett.* **293**, 163 (2000).
4. L. Manuelidis, Z. Y. Lu, *Proc. Natl. Acad. Sci. U.S.A.* **100**, 5360 (2003).
5. A. Dickinson, H. Fraser, V. Meikle, G. Outram, *Nature New Biol.* **237**, 244 (1972).
6. C. Baker, L. Manuelidis, *Proc. Natl. Acad. Sci. U.S.A.* **100**, 675 (2003).
7. C. Baker, Z. Lu, L. Manuelidis, *J. Neurovirol.* **10**, 1 (2004).
8. Z. Lu, C. Baker, L. Manuelidis, *J. Cell. Biochem.* **93**, 644 (2004).
9. N. Nishida *et al.*, *J. Virol.* **74**, 320 (2000).
10. A. Arjona, L. Simarro, F. Islinger, N. Nishida, L. Manuelidis, *Proc. Natl. Acad. Sci. U.S.A.* **101**, 8768 (2004).
11. See supporting data on *Science* Online.
12. C. Lasmezas *et al.*, *Science* **275**, 402 (1997).
13. Y. G. Xi, A. Ingrosso, A. Ladogana, C. Masullo, M. Pocchiari, *Nature* **356**, 598 (1992).
14. A. Hill *et al.*, *Brain* **126**, 1333 (2003).
15. L. Manuelidis *et al.*, *J. Virol.* **74**, 8614 (2000).
16. S. Prusiner, *Proc. Natl. Acad. Sci. U.S.A.* **95**, 13363 (1998).
17. G. S. Jackson, J. Collinge, *Mol. Pathol.* **54**, 393 (2001).
18. T. Sklaviadis, R. Dreyer, L. Manuelidis, *Virus Res.* **3**, 241 (1992).
19. L. Manuelidis, T. Sklaviadis, A. Akowitz, W. Fritch, *Proc. Natl. Acad. Sci. U.S.A.* **92**, 5124 (1995).
20. A. Barrett, *Curr. Top. Microbiol. Immunol.* **128**, 55 (1986).
21. J. Wu *et al.*, *World J. Gastroenterol.* **11**, 1658 (2005).
22. P. M. Waterhouse, M. B. Wang, T. Lough, *Nature* **411**, 834 (2001).
23. L. Manuelidis, in *Transmissible Subacute Spongiform Encephalopathies: Prion Diseases*, L. Court, B. Dodet, Eds. (Elsevier, Paris, 1966), pp. 375–387.
24. L. Manuelidis *et al.*, unpublished data.
25. L. Linsell *et al.*, *Neurology* **63**, 2077 (2004).
26. P. Smith, S. Cousens, J. d'Huillard Aignaux, H. Ward, R. Will, *Curr. Top. Microbiol. Immunol.* **284**, 161 (2004).

27. Supported by NIH grant NS12674, U.S. Department of Defense grant DAMD-17-03-1-0360, and a grant from the Ministry of Health, Labor and Welfare, Japan.

Supporting Online Material

www.sciencemag.org/cgi/content/full/310/5747/493/DC1

Materials and Methods

29 July 2005; accepted 21 September 2005

10.1126/science.1118155

Interlinked Fast and Slow Positive Feedback Loops Drive Reliable Cell Decisions

Onn Brandman,[1,2]* James E. Ferrell Jr.,[1] Rong Li,[2,3,4] Tobias Meyer[1,2]

Positive feedback is a ubiquitous signal transduction motif that allows systems to convert graded inputs into decisive, all-or-none outputs. Here we investigate why the positive feedback switches that regulate polarization of budding yeast, calcium signaling, *Xenopus* oocyte maturation, and various other processes use multiple interlinked loops rather than single positive feedback loops. Mathematical simulations revealed that linking fast and slow positive feedback loops creates a "dual-time" switch that is both rapidly inducible and resistant to noise in the upstream signaling system.

Studies in many biological systems have identified positive feedback as the key regulatory motif in the creation of switches with all-or-none "digital" output characteristics (*1*). Although a single positive feedback loop (*A* activates *B* and *B* activates *A*) or the equivalent double-negative feedback loop (*A* inhibits *B* and *B* inhibits *A*) can, under the proper circumstances, generate a bistable all-or-none switch (*1*–*5*), it is intriguing that many biological systems have not only a single but multiple positive feedback loops (Table 1). Three examples of positive feedback systems are shown in more detail in Fig. 1.

[1]Department of Molecular Pharmacology, Stanford University School of Medicine, Stanford, CA, 94305, USA. [2]Physiology Course 2004, Marine Biological Laboratory, Woods Hole, MA 02543, USA. [3]Department of Cell Biology, Harvard Medical School, Boston, MA 02115, USA. [4]The Stowers Institute for Medical Research, Kansas City, MO 64110, USA.

*To whom correspondence should be addressed. E-mail: onn@stanford.edu

Polarization in budding yeast depends on two positive feedback loops, a rapid loop involving activity cycling of the small guanosine triphosphatase Cdc42 and a slower loop that may involve actin-mediated transport of Cdc42 (Fig. 1A) (*6*). In many cell types, the induction of prolonged Ca^{2+} signals involves initial rapid positive feedback loops centered on Ca^{2+} release mediated by inositol 1,4,5-trisphosphate (IP3) combined with a much slower loop that induces Ca^{2+} influx mediated by the depletion of Ca^{2+} stores (*7*, *8*) (Fig. 1B). *Xenopus* oocytes respond to maturation-inducing stimuli by activating a rapid phosphorylation/dephosphorylation–mediated positive feedback loop (between Cdc2, Myt1, and Cdc25) and a slower translational positive feedback loop [between Cdc2 and the the mitogen-activated protein kinase (MAPK or ERK) cascade, which includes Mos, MEK (MAPK kinase), and p42] (Fig. 1C).

The presence of multiple interlinked positive loops raises the question of the performance

JOURNAL OF VIROLOGY, June 2005, p. 7104–7112 Vol. 79, No. 11
0022-538X/05/$08.00+0 doi:10.1128/JVI.79.11.7104–7112.2005

Biological and Biochemical Characteristics of Prion Strains Conserved in Persistently Infected Cell Cultures

Kazuhiko Arima,[1] Noriyuki Nishida,[1] Suehiro Sakaguchi,[1,3] Kazuto Shigematsu,[2] Ryuichiro Atarashi,[1] Naohiro Yamaguchi,[1] Daisuke Yoshikawa,[1] Jaewoo Yoon,[1] Ken Watanabe,[1] Nobuyuki Kobayashi,[1] Sophie Mouillet-Richard,[4] Sylvain Lehmann,[5] and Shigeru Katamine[1]*

Department of Molecular Microbiology and Immunology,[1] and Department of Pathology 2,[2] Nagasaki University Graduate School of Biomedical Sciences, Sakamoto 1-12-4, Nagasaki 852-8523, Japan; PRESTO, Japan Science and Technology Agency, 4-1-8 Honcho Kawaguchi, Saitama, Japan [3]; Institut André Lwoff, CNRS UPR 1983-BP8, 94801 Villejuif Cedex, France[4]; and Institut de Genetique Humaine, CNRS UPR 1142, 34396 Montpellier Cedex 5, France[5]

Received 16 August 2004/Accepted 18 January 2005

Abnormal prion protein (PrP^{Sc}) plays a central role in the transmission of prion diseases, but the molecular basis of prion strains with distinct biological characteristics remains to be elucidated. We analyzed the characteristics of prion disease by using mice inoculated with the Chandler and Fukuoka-1 strains propagated in a cultured mouse neuronal cell line, GT1-7, which is highly permissive to replication of the infectious agents. Strain-specific biological characteristics, including clinical manifestations, incubation period as related to the infectious unit, and pathological profiles, remained unchanged after passages in the cell cultures. We noted some differences in the biochemical aspects of PrP^{Sc} between brain tissues and GT1-7 cells which were unlikely to affect the strain phenotypes. On the other hand, the proteinase K-resistant PrP core fragments derived from Fukuoka-1-infected tissues and cells were slightly larger than those from Chandler-infected versions. Moreover, Fukuoka-1 infection, but not Chandler infection, gave an extra fragment with a low molecular weight, ~13 kDa, in both brain tissues and GT1-7 cells. This cell culture model persistently infected with different strains will provide a new insight into the understanding of the molecular basis of prion diversity.

Transmissible spongiform encephalopathies (TSEs) are a series of neurodegenerative disorders that include Creutzfeldt-Jakob disease (CJD), Gerstmann-Straussler-Scheinker syndrome (GSS), and fatal familial insomnia in humans and bovine spongiform encephalopathy and scrapie in animals (23, 25). Human TSEs may have infectious, sporadic, or genetic origins, but the brain tissues from affected individuals always possess an infectious agent, termed prion, capable of transmitting the disease to laboratory animals. The protein-only hypothesis proposes that the abnormal isoform of the prion protein (PrP^{Sc}) accumulated via posttranslational modification of the cellular isoform (PrP^{C}) is the sole component of the infectious particle (25). In fact, while the agent is extremely resistant to inactivation by UV and ionizing radiation, protein denaturants can abolish the infectivity, and moreover, no specific genetic materials for infectious agents have been identified. The two PrP isoforms are distinguishable by their biochemical properties. PrP^{C} is readily soluble in nondenaturing detergents and completely digested by proteinase K (PK), whereas PrP^{Sc} is detergent insoluble and resistant to proteolysis except for the N-terminal region comprising ~67 residues. Structural studies have suggested that the former is rich in alpha-helical structures with small β-sheet regions, but the latter has a high β-sheet content. The central role of PrP in the diseases is exemplified by the fact that PrP-null mice are resistant to the disease (6, 27), by the causal linkage of genetic forms of human TSEs with mutation in the PrP gene (25), and by the dependency of the species barriers on the primary PrP sequences (29). The existence of strain variation, however, has challenged the protein-only hypothesis. Individual infectious agents have been shown to maintain their phenotypic characteristics, including the clinical presentation of disease, the length of the incubation period, and the distribution of vacuolar degeneration and PrP^{Sc} deposition in the central nervous system (CNS) during serial transmission between same-species animals. In addition to these biological characteristics, biochemical differences in PrP^{Sc} have been reported. Transmission of two different inherited human prion diseases, fatal familial insomnia and familial CJD, to mice resulted in the accumulation of PrP^{Sc} with PK-resistant core fragments with molecular masses of 19 and 21 kDa, respectively (35). The difference in the size of PK-resistant PrP^{Sc} fragments has been also documented among agents originating from scrapie and mink spongiform encephalopathies (3). The degree of glycosylation is also proposed to be an important signature of some strains. There are two sites of Asn-linked glycosylation at the C-terminal portion, and the degree of glycosylation is thus represented by the ratio of three glycoforms, di-, mono-, and unglycosylated forms. The unique PrP^{Sc} glycoform pattern, in which the diglycosylated form dominates, in animals and patients affected with bovine spongiform encephalopathy and variant CJD, respectively, is distinct from those of other known strains (11) with a few exceptions (32). Because diversity in the size of a PK-resistant PrP core fragment and the degree of its Asn-linked glycosylation were thought to be consequences of differences in the conformation, it has been hypothesized that strain-specific conformations of PrP^{Sc} could determine the strain phenotype.

* Corresponding author. Mailing address: Department of Molecular Microbiology and Immunology, Nagasaki University Graduate School of Biomedical Sciences, Sakamoto 1-12-4, Nagasaki 852-8523, Japan. Phone: 81-95-849-7057. Fax: 81-95-849-7060. E-mail: katamine@net.nagasaki-u.ac.jp.

However, the strain-specific conformation of PrP^{Sc} and, in particular, its causal relationship with strain phenotypes, still remains controversial (13, 21).

Most of the information regarding strains so far available has been obtained from in vivo experiments using mice or hamsters, a system less advantageous for biochemical approaches to the molecular mechanisms of the strains. Neuronal cell culture models are clearly of greater value for such studies. However, only a few cultured cell lines, including PC12 and mouse neuroblastoma-derived N2a, have been shown to be permissive to scrapie agents (7, 26), and the levels of replication in these cell lines are not satisfactory, at least for quantitative detection of infectivity. Some of us previously demonstrated that cultured mouse neuronal cells expressing a high amount of PrP^{C} were highly permissive to replication of various mouse-adapted strains (15, 18). Arjona et al. recently compared two CJD strains using GT1-7 and N2a58 cells (1). The aim of the present study was to confirm the usefulness of the neuronal cell culture models by comparing phenotypes of mice inoculated with two strains, Chandler and Fukuoka-1. We report here that passage through the cell cultures did not change the strain-specific nature of the biological characteristics and discuss the relationship between strain phenotype and biochemical aspects of the PrP.

MATERIALS AND METHODS

Cell cultures. The mouse neuronal cell line GT1-7 (14) was exposed to mouse brain homogenates infected with each prion strain as described previously (15, 16, 18). The cells were cultured in DMEM containing heat-inactivated fetal bovine serum at 10% and penicillin-streptomycin and split every 5 days at a 1:3 ratio. All cultured cells were maintained at 37°C in 5% CO_2 in the biohazard prevention area of the authors' institution.

Mice. ddY mice used in the experiments were fed under specific-pathogen-free conditions. Experiments involving agent inoculation were conducted in the biohazard prevention area (P3) of the Laboratory Animal Center for Biomedical Research of the authors' institution.

Prion strains. The Fukuoka-1 strain (34) was passaged three times in the brains of ddY mice. The brains infected with Chandler strains were kindly donated by B. Caughey and R. Carp, respectively. The pooled brains were homogenized to 1% (wt/vol) in cold phosphate-buffered saline (PBS) containing 5% glucose. Cultured cell lysates were prepared by sonication in PBS. All of the homogenates and cell lysates were kept at −80°C until use.

Determination of LD_{50}. Confluent cell cultures in a 100-mm dish (approximately 7.5×10^6 cells) were sonicated in 0.5 ml of PBS. Before use, the cells were cultured for more than 30 passages following the initial ex vivo challenges. The cultured cell lysates and 1% (wt/vol) homogenates of brain tissues were serially diluted 10-fold with PBS, from 10^0 to 10^{-6}, and 20 μl of each dilution was inoculated into the right brain (five mice for each group). The inoculated mice were observed until 364 days after inoculation. The onset of disease was determined as previously described (28). The 50% lethal dose (LD_{50}) was determined according to the Behrens-Karber formula (10).

Histology. The brains were fixed in 4% paraformaldehyde and sectioned into 7-μm-thick sections at levels 250 and 500, as described by Sidman et al. (30). The tissue sections were stained with hematoxylin and eosin. The pattern of vacuolation was examined in 9 areas, namely the midbrain, hypothalamus, thalamus, hippocampus, paraterminal body, posterior cortex, cerebellar medulla, cerebellar granular layer, and cerebellar molecular layer. The vacuolation score was established based on the pattern, size, and density of the vacuoles using standard criteria from grade 0 for none and grade 5 for maximum vacuolation (9)

Antibodies. The anti-PrP polyclonal mouse antiserum used was described previously (19). The IBL-N rabbit antibody against N-terminal peptides of PrP and M20 goat antibody to C-terminal PrP peptides were purchased from Immuno Biological Laboratories (Gunma, Japan) and Santa-Cruz Biotech (Santa Cruz, CA), respectively. Horseradish peroxidase (HRP)-conjugated anti-mouse and -rabbit immunoglobulin G antibodies were purchased from Amersham. HRP-conjugated anti-goat immunoglobulin G antibodies were purchased from Santa-Cruz Biotech.

Immunoblotting. Confluent cultures were lysed for 30 min at 4°C in Triton-DOC lysis buffer (50 mM Tris-HCl [pH 7.5] containing 150 mM NaCl, 0.5% Triton X-100, 0.5% sodium deoxycholate, and 2 mM EDTA). After 1 min of centrifugation at $500 \times g$, the supernatant was collected and its total protein concentration was measured using the Bio-Rad protein assay. To detect PrP^{Sc}, the brain homogenates and cell lysates, with the protein concentration adjusted to 10 mg/ml, were treated with 100 μg/ml of proteinase K (Sigma) at 37°C for 30 min. To remove N-linked glycosylation, PNGase F was used according to the manufacturer's protocol (New England Biolabs) before PK digestion. The samples were boiled for 5 min in sodium dodecyl sulfate (SDS) loading buffer (50 mM Tris-HCl, pH 6.8, containing 5% glycerol, 1.6% SDS, and 100 mM dithiothreitol) and subjected to SDS–12% polyacrylamide gel electrophoresis. The proteins were transferred onto an Immobilon-P membrane (Millipore) in transfer buffer containing 15% methanol at 400 mA for 60 min, and the membrane was blocked with 5% nonfat dry milk in TBST (10 mM Tris-HCl [pH 7.8], 100 mM NaCl, 0.1% Tween 20) for 1 h at room temperature and reacted with anti-PrP antibodies. Immunoreactive bands were visualized by HRP-conjugated secondary antibodies using an enhanced chemiluminescence system (ECL; Amersham Pharmacia Biotech).

RESULTS

Biological characteristics of prion strains in cultured cells: clinical signs in inoculated mice. To examine the biological characteristics of the Chandler and Fukuoka-1 prion strains, GT1-7 cells independently infected with the two strains as well as infected mouse brain homogenates were inoculated into the brains of ddY mice. As shown in Table 1, all of the homogenates produced neurological symptoms and subsequent death in the inoculated mice. They exhibited some common clinical signs, such as weight loss, ruffled and greasy yellowish hair, tremor, hypersensitivity to sound and touch, and locomotor disturbance. However, all of the Chandler-infected mice were hyperactive at the early stages of the disease, in contrast to the progressive hypoactivity of Fukuoka-1-infected mice. When the mice at the terminal stages were sacrificed, a markedly extended bladder, due to urination disturbance, was observed in Fukuoka-1-inoculated, but not Chandler-inoculated, mice. These strain-specific symptoms were reproduced without exception in all of the mice, irrespective of whether brain homogenates or cultured cell lysates were used.

Incubation periods in inoculated mice. As shown in Table 1, the incubation periods of the mice inoculated with 1% brain homogenates of Fukuoka-1 and Chandler were 128.6 ± 9.9 days (mean ± standard deviation) and 149.8 ± 4.4 days, respectively. Interestingly, GT1-7 cells infected with Fukuoka-1 also exhibited a shorter incubation period than Chandler-infected cells: 139.7 ± 12.5 versus 150.2 ± 5.9 days. To analyze more quantitatively, the brain homogenates and GT1-7 cell lysates infected with Fukuoka-1 and Chandler, designated Fukuoka-1/brain, Chandler/brain, Fukuoka-1/GT1-7, and Chandler/GT1-7, respectively, were subjected to the end-point 10-fold dilution assay (Table 1). According to Behrens and Korber's formula, the infectious titers were estimated to be $10^{8.1}$ and $10^{8.8}$ LD_{50} units/g of the brain tissues and $10^{5.3}$ and $10^{6.5}$ LD_{50} units/10^7 GT1-7 cells infected with Fukuoka-1 and Chandler, respectively. After each dilution was converted to its infectious titer, the relationships between infectious titers and incubation periods in the four materials were analyzed. As shown in Fig. 1, plots of Fukuoka-1/brain and Fukuoka-1/GT1-7 clustered in the same region, and those of Chandler/brain and Chandler/GT1-7 formed another cluster located at the region representing much longer incubation periods. The linear relationships between infectious titers and incubation periods in brain homogenates and cell lysates in-

TABLE 1. Mortality and incubation periods of mice inoculated with prion strains[a]

Tissue or cell type	Fukuoka-1 strain			Chandler strain		
	Dilution	Mortality (no. dead/total)	Incubation period (days ± SD)	Dilution	Mortality (no. dead/total)	Incubation period (days ± SD)
Brain homogenate[b]	10^{-2}	5/5	128.6 ± 9.9	10^{-2}	5/5	149.8 ± 4.7
	10^{-3}	5/5	139.2 ± 8.9	10^{-3}	5/5	155.4 ± 7.1
	10^{-4}	5/5	145.6 ± 11.4	10^{-4}	5/5	183.4 ± 8.0
	10^{-5}	4/5	184.7 ± 25.7	10^{-5}	5/5	193.4 ± 16.8
	10^{-6}	4/5	250.5 ± 57.4	10^{-6}	3/5	204.0 ± 27.7
	10^{-7}	1/5	230.0	10^{-7}	4/5	248.0 ± 37.4
	10^{-8}	0/5		10^{-8}	0/5	
	10^{-9}	ND[d]		10^{-9}	0/5	
GT1-7 cell lysate[c]	10^{-0}	4/4	139.7 ± 12.5	10^{-0}	4/4	150.2 ± 5.9
	10^{-1}	5/5	137.2 ± 12.6	10^{-1}	4/4	167.3 ± 11.8
	10^{-2}	5/5	152.4 ± 10.0	10^{-2}	5/5	174.0 ± 10.5
	10^{-3}	5/5	199.4 ± 58.7	10^{-3}	5/5	193.6 ± 13.7
	10^{-4}	2/5	211.0 ± 4.2	10^{-4}	4/5	205.7 ± 18.5
	10^{-5}	0/5		10^{-5}	2/5	203.5 ± 27.5
	10^{-6}	0/5		10^{-6}	2/5	275.5 ± 71.4
	10^{-7}	0/5		10^{-7}	0/5	

[a] Twenty-microliter aliquots of serial 10-fold dilutions of GT1-7 cell lysates and brain homogenates (10^2, 1% [wt/vol] homogenate) were inoculated into the brain of a mouse. Inoculated cells were passaged 35 times before use.
[b] Infectious titers of the brain tissues infected with Fukuoka-1 and Chandler were $10^{8.1}$ and $10^{8.8}$ LD_{50} units/g tissue, respectively.
[c] Infectious titers of Fukuoka-1 and Chandler-infected GT1-7 cells were $10^{6.3}$ and $10^{6.5}$ LD_{50} units/10^7 cells, respectively.
[d] ND, not defined.

fected with each strain overlapped but were distinct between the strains (Fig. 1).

Pathological findings in inoculated mice. Brain sections including the hippocampus, thalamus, and cerebellum from inoculated mice at the terminal stage were stained with hematoxylin and eosin. As shown in Fig. 2, although spongiform change, neuronal loss, and gliosis are common characteristics of prion diseases, the severity and distribution of histological abnormalities differed between the brain tissues of Fukuoka-1- and Chandler-infected mice. In the Fukuoka-1-infected brains, large empty vacuoles were prominent mainly in the white matter, and a microcystic structure measuring up to 100 μm in diameter was observed in the cerebellar medulla (Fig. 2a and e). The grey matter was also affected in advanced cases, while the cerebellar granular and molecular layers were not damaged. The vacuoles in Chandler strain-infected brains were distributed equally in the grey and white matter. However, the number of vacuoles was fewer, and the size, an average of 27 μm in diameter, was obviously smaller than that of those from Fukuoka-1 strain-infected brains (Fig. 2b and f). In general, histopathological changes were much more severe in Fukuoka-1-infected tissues compared with those infected with the Chandler strain. These strain-specific pathological profiles were reproduced by inoculation of GT1-7 cell lysates infected with either strain (Fig. 2c, d, g, and h). A semiquantitative evaluation of the number and size of vacuoles (vacuolation score) in selected areas of brain tissues confirmed that the lesion profiles were strain specific (Fig. 3).

Biochemical aspects of PrP. Biochemical characteristics of PrP in the noninfected brain tissues and GT1-7 cells were

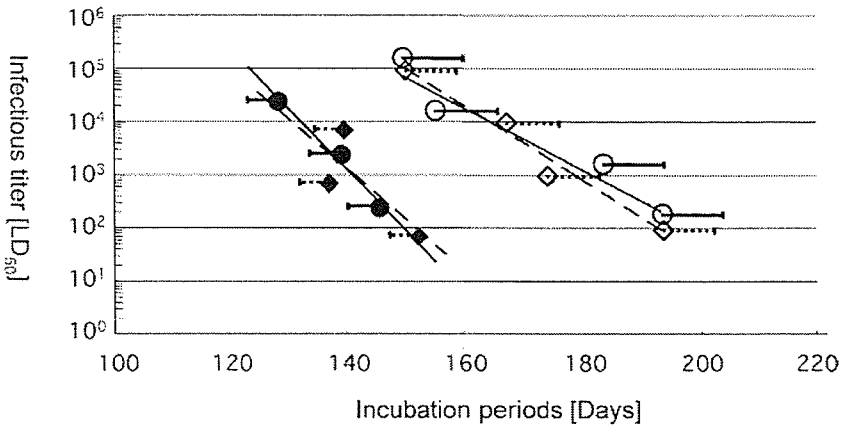

FIG. 1. Linear relationship between infectious titers and incubation periods. Each dilution used in the end-point assay shown in Table 1 was converted to its infectious titer, and the relationships between infectious titers (LD_{50}) and incubation periods (days) in Fukuoka-1/brain (closed circles), Chandler/brain (open circles), Fukuoka-1/GT1-7 (closed squares), and Chandler/GT1-7 (open squares) were analyzed. Horizontal bars indicate standard deviations.